nature physics

ARTICLES

https://doi.org/10.1038/s41567-020-01149-0

Observation of a marginal Fermi glass

Fahad Mahmood[1,2,3]✉, Dipanjan Chaudhuri[1], Sarang Gopalakrishnan[4,5], Rahul Nandkishore[6] and N. P. Armitage[1]✉

A long-standing open problem in condensed-matter physics is whether or not a strongly disordered interacting insulator can be mapped to a system of effectively non-interacting localized excitations. Using terahertz two-dimensional coherent spectroscopy, we investigate this issue in phosphorus-doped silicon, a classic example of a correlated disordered electron system in three dimensions. Despite the intrinsically disordered nature of these materials, we observe coherent excitations and strong photon echoes that provide us with a powerful method for the study of their decay processes. We extract the energy relaxation and decoherence rates close to the metal–insulator transition. We observe that both rates are linear in excitation frequency with a slope close to unity. The energy relaxation timescale counterintuitively increases with increasing temperature, and the coherence relaxation timescale has little temperature dependence below 25 K, but increases as the material is doped towards the metal–insulator transition. Here we argue that these features imply that the system behaves as a well-isolated electronic system on the timescales of interest, and relaxation is controlled by electron–electron interactions. Our observations constitute a distinct phenomenology, driven by the interplay of strong disorder and strong electron–electron interactions, which we dub the marginal Fermi glass.

Understanding systems with strong disorder and strong interactions is a central problem in condensed-matter physics. It is a remarkable fact that many metals can be understood in terms of weakly interacting fermionic quasiparticles near the Fermi energy (E_F), despite the fact that the bare Coulomb interaction is not particularly small or short-ranged. This has been canonized in terms of Landau Fermi liquid theory[1], where the effects of interactions renormalize quasiparticle parameters like the effective mass, but do not change the underlying effective structure of the theory from that of free electrons. The scattering rates of quasiparticles in a Landau Fermi liquid go like $(E - E_F)^2$, so quasiparticles are arbitrarily well-defined near E_F. These effects arise as a consequence of both the Pauli exclusion principle, which reduces the phase space for scattering, and screening, which renders the bare Coulomb interaction effectively short-range.

The tendency of strong disorder is to localize particles. Anderson showed that, in the absence of interactions, sufficiently strong disorder could localize wavefunctions with a sharp boundary in energy between localized and extended states[2]. This is a generic wave phenomenon that applies equally to acoustic, electromagnetic or neutral matter waves[3]. Although such 'Anderson localization' is frequently invoked in the study of disordered electronic insulators, it is unclear to what extent this phenomenon actually applies to real materials.

In this regard, in 1970 Anderson proposed the notion—in analogy with the Fermi liquid—of a 'Fermi glass' as a localized disordered state of matter adiabatically connected to the non-interacting Anderson insulator, whose universal properties arose through Pauli exclusion alone[4]. Anderson conjectured that, via the protection afforded by the Fermi energy, such a state of matter would also have well-defined single-particle-like excitations at low energy. It was later understood that the localized nature of such systems and lack of metallic screening made these considerations more subtle[5–7]. Recently, it was realized that insulators might feature an even stronger notion of adiabatic continuity than metals. It is argued in refs. [8,9] that a disordered system with short-range interactions could be 'many-body-localized' and thus have infinitely sharp excitations, even at non-zero temperatures and far from E_F. This has been a large area of current investigation (see refs. [10,11] for reviews). However the effects of long-range Coulomb interactions are still not fully understood. It has been shown[12–15] that long-range interactions invalidate perturbative arguments for localization. Although non-perturbative methods have been applied in certain settings[16], it remains unknown whether a 'Fermi glass' exists, that is, whether a frequency or temperature window exists where the excitations of an interacting insulator are renormalized, weakly interacting, electron-like quasiparticles.

In this Article, we use the technique of terahertz two-dimensional coherent spectroscopy (THz 2DCS)[17–19] to shed light on this fundamental problem. We investigate the canonical disordered material phosphorus-doped silicon (Si:P) on the insulating side of the metal–insulator transition (MIT)[20,21]. Among other aspects, THz 2DCS allows us to measure both the T_1 and T_2 times (the longitudinal and transverse relaxation times, respectively) of inhomogeneously broadened spectra in the terahertz range. At low temperature we find a temperature-independent regime governed by electron–electron interactions. We find that relaxation rates of the optical excitations are linear in frequency with a proportionality constant of order one. This establishes that, in our frequency range, the low energy excitations are not well defined. This is consistent with a picture in which localized electronic systems are not adiabatically connected to the Anderson insulator. We call this state of matter the 'marginal Fermi glass'. This electronic relaxation is consistent with the existence of an electronic continuum that arises through long-range Coulomb interactions, which could destabilize the localized state at non-zero temperatures.

[1]Department of Physics and Astronomy, The Johns Hopkins University, Baltimore, MD, USA. [2]Department of Physics, University of Illinois at Urbana-Champaign, Urbana, IL, USA. [3]F. Seitz Materials Research Laboratory, University of Illinois at Urbana-Champaign, Urbana, IL, USA. [4]Department of Engineering Science and Physics, CUNY College of Staten Island, Staten Island, NY, USA. [5]Initiative for Theoretical Sciences, The Graduate Center, CUNY, New York, NY, USA. [6]Department of Physics and Center for Theory of Quantum Matter, University of Colorado Boulder, Boulder, CO, USA.
✉e-mail: fahad@illinois.edu; npa@jhu.edu

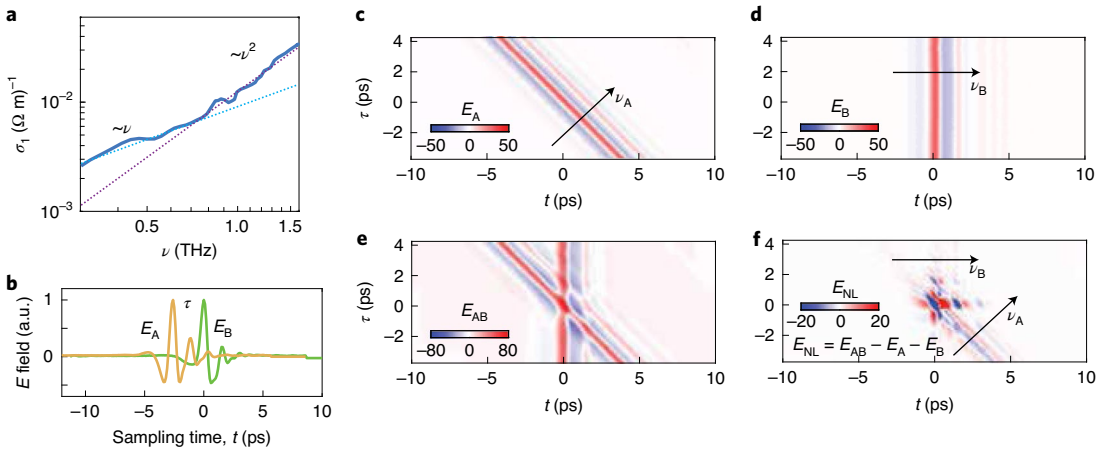

Fig. 1 | Linear and nonlinear optical response of phosphorus-doped silicon. a, Linear-response optical conductivity for the 39% sample at 5 K. Regimes of linear and quadratic power-law behaviour can be distinguished (dashed lines). **b**, Time traces of two collinear terahertz pulses that are separated by a time τ. In the experiment, the sum of these electric fields, E_{AB}, is measured. **c**–**f**, Time traces of E_A (**c**), E_B (**d**), E_{AB} (**e**) and $E_{NL} = E_{AB} - E_A - E_B$ (**f**) as a function of t and τ.

Figure 1a presents the real part of the linear-response, terahertz-range conductivity of a representative 39% doped sample. In previous work[22,23] it was shown that the optical response of Si:P near the MIT was in accord with the theory of Mott–Efros–Shklovskii[24,25]. The excited states of the system are modelled as an ensemble of resonant pairs that can be mapped to a random ensemble of two-level systems (that is, the 'pair approximation'), which gives a conductivity $\sigma_1(\omega) = \alpha e^2 N_0^2 \xi^5 \omega [\ln(2I_0/\hbar\omega)]^4 [\hbar\omega + U(r_w)]$; for example, an almost linear conductivity is found at low frequencies and a quadratic one at higher frequencies. These power laws come from phase space considerations (Supplementary Section IV). They cross over at an energy scale of $U(r_\omega) = e^2/\varepsilon_1 r_\omega$, which represents the attraction between an electron and hole in a dipolar excitation at a distance $r_\omega = \xi[\ln(2I_0/\hbar\omega)]$. Here, N_0 is the density of states, ξ is the localization length, ε_1 is the full dielectric constant, α is a constant close to one and I_0 is the pre-factor of the overlap integral (commonly taken to be the Bohr energy of the dopant). One aspect not considered in the usual treatment is that each of the excitations that contributes to $\sigma(\omega)$ has a finite lifetime. The functional form of $\sigma(\omega)$ is insensitive to moderate level broadening, so it is uninformative about excitation lifetimes. Quantifying homogeneous broadening due to quasiparticle decay in the face of overtly inhomogeneously broadened spectra is the principal difficulty in characterizing interactions in these systems.

Two-dimensional coherent spectroscopy is a nonlinear four-wave mixing technique that can, among other aspects, directly reveal couplings between excitations and separate homogeneous from inhomogeneous broadening[26–29]. It has been incredibly powerful in its radio and infrared frequency incarnations for the study of chemical systems. It has been extended recently to the terahertz range to study graphene and quantum wells[17,30], molecular rotations[31] and spin waves in conventional magnets[18]. It has also been proposed to give unique information about fractionalized spin phases[19,32].

As discussed in the Methods, two terahertz pulses (A and B) are incident on a sample. The transmitted electric field is recorded as a function of the separation between them (τ) and the time from pulse B (t). The nonlinear signal is defined as $E_{NL}(\tau,t) = E_{AB}(\tau,t) - E_A(\tau,t) - E_B(t)$, where E_{AB} is the transmitted signal when both terahertz pulses are present, and E_A and E_B are the transmitted signals with each pulse A and B present individually. Figure 1c–f shows E_A, E_B, E_{AB} and E_{NL} as a function of t and τ for the 39% sample. Figure 2 shows the resulting 2D terahertz spectra $E_{NL}(\nu_\tau,\nu_t)$ from the Fourier transforms with respect to τ and t for each doping, studied at a temperature of 5 K. We note that typical P–P spacings in these samples are of order 8 nm (ref. [22]), so the associated Coulomb energy is of order 15 meV, which corresponds to a timescale of ~0.3 ps. The experimental timescales of these measurements of a few picoseconds are thus easily long enough for the effect of interactions to be important. The key results were verified to be insensitive to the incident fluence, thus establishing that heating effects are minimal (Supplementary Section II).

In an inversion symmetric system like Si:P, the leading nonlinear response is $\chi^{(3)}$ electric dipole reradiation. With two pulses, there are thus contributions to E_{NL} in which pulse A interacts twice and pulse B once with the sample, and other contributions where pulse A interacts once and pulse B twice. Moreover, the $\chi^{(3)}$ response can be separated into non-rephasing (NR) and rephasing (R) contributions[17,18]. The R signal arises due to a reverse phase accumulation during time t compared with τ and thus occurs at negative frequencies of either ν_t or ν_τ when compared with the NR signal. The different nonlinear signals in each quadrant in the 2D frequency plan can be understood in terms of 'frequency vectors', as outlined in refs. [17,19] and Supplementary Section III. For the case where pulse A precedes B and pulse B has two sample interactions (AB scheme), the E_{NL} signal in the fourth quadrant is the 'photon echo' R contribution. Within a picture where excitations are resonant pairs, its anti-diagonal widths are a measure of the decoherence rates ($\Gamma_2 = 1/T_2$)[26,27,33]. The strong signal along the diagonal in the first quadrant is a pump–probe (PP) contribution from pulse B interacting twice from the sample and arriving before A (BA scheme). It is sensitive to decay of the excited-state populations and its anti-diagonal width is, within the pair approximation, a measure of the energy relaxation rate ($\Gamma_1 = 1/T_1$) at the excitation frequency of the projection onto either axis. See Supplementary Section III for a detailed description of the full 2DCS response of a generic two-level system subject to finite longitudinal and transverse relaxation rates $1/T_1$ and $1/T_2$.

As can be seen in Fig. 2, the signals shift towards lower frequencies on approaching the MIT. The echo signal is most apparent for the least-doped (39%) sample (Fig. 2a). Similarly, the PP streak along the first quadrant diagonal narrows (decreasing Γ_1) with increasing doping. To quantify the relaxation rates $\Gamma_{1,2}$, we take cuts along the anti-diagonal in both quadrants. In so doing, we can obtain the relaxation rates as a function of energy. Figure 3a shows representative cuts of the 39% sample taken along the green and purple dashed lines in Fig. 2a. The cuts in each case can be well fit

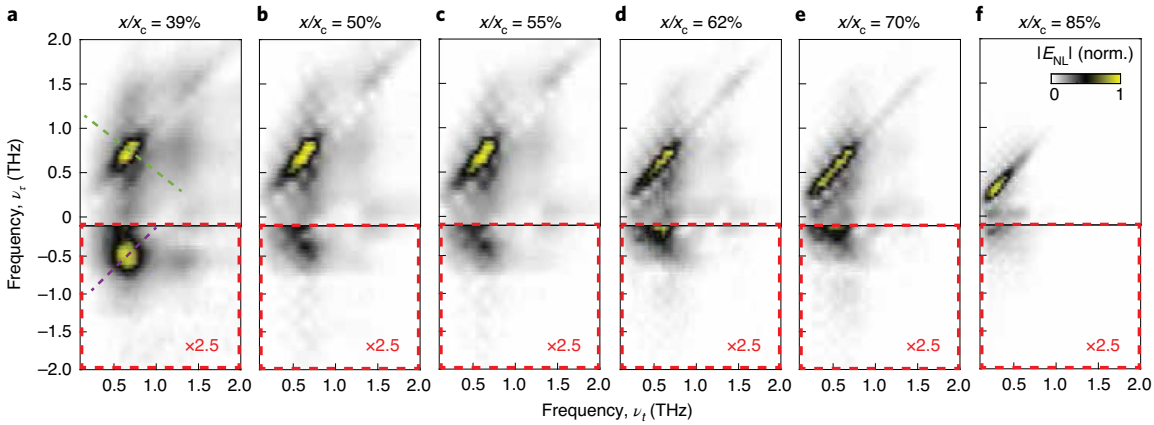

Fig. 2 | Two-dimensional terahertz spectra at different phosphorus concentrations. a–f, Two-dimensional terahertz spectra $|E_{NL}(\nu_\tau, \nu_t)|$ at $T = 5$ K for a series of Si:P samples with different dopings (x/x_c): 39% (**a**), 50% (**b**), 55% (**c**), 62% (**d**), 70% (**e**) and 85% (**f**). The doping for each sample is expressed as a percent of the critical doping (x_c) at which the MIT occurs. The spectra are obtained by taking the absolute value of the 2D Fourier transform of the time-domain signal $E_{NL}(t, \tau)$. The spectrum at each doping is normalized to its maximum and plotted according to the colour map shown in **f**. The intensity in the fourth quadrant (red dashed area) from which we get Γ_2 is magnified by ×2.5.

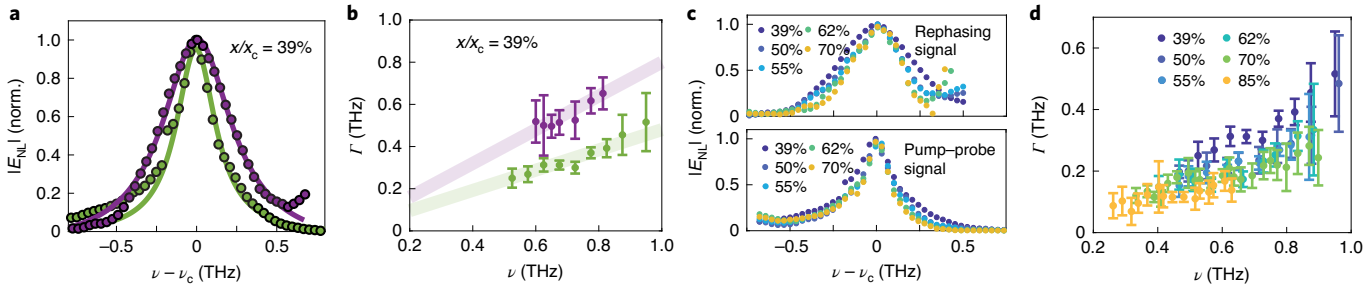

Fig. 3 | Frequency and doping dependence of the pump–probe and rephasing relaxation rates. a, $|E_{NL}|$ as a function of excitation frequency along the anti-diagonal cuts indicated by the dashed green and purple lines in Fig. 2a for the 39% sample at 5 K. Green dots are cut through the first-quadrant PP signal, while purple dots represent a cut through the fourth-quadrant R signal. The solid lines show a Lorentzian best fit to the data. **b**, As discussed in Supplementary Section III, the widths of these two features can be interpreted as $\Gamma_1 = 1/T_1$ (green dots) and $\Gamma_2 = 1/T_2$ (purple dots) within a model of two-level systems. Γ_1 and Γ_2 are shown as a function of excitation frequency for the 39% sample. Solid lines extrapolate through the origin and are a linear best fit guide to the eye. **c**, $|E_{NL}|$ as a function of excitation frequency along the anti-diagonal direction at $\nu_t = 0.67$ THz for different dopings. The top panel shows cuts through the fourth-quadrant R signal, and the bottom panel shows cuts through the first-quadrant PP signal. **d**, Γ_1 as a function of frequency at different dopings at 5 K. Error bars in **b** and **d** represent the 95% confidence interval in the Lorentzian best fit.

to a single Lorentzian to extract the full-width at half-maximum as a measure of the relaxation rates. We plot the frequency dependencies of the relaxation rates in Fig. 3b and the doping dependencies in Fig. 3c. The relative widths of $\Gamma_{1,2}$ easily satisfy the fundamental relation for 'magnetic' resonance with $2/T_2 \geq 1/T_1$. The frequency dependence of Γ_1 is shown in Fig. 3d at different doping levels. Note that the x axes in Fig. 3b,d show the frequency ν_t at which the anti-diagonal cuts peak in Fig. 2. Because of the low signal, it was challenging to extract Γ_2 over the full doping range for all samples.

One can see in Fig. 3b,d that the relaxation rates are roughly linear in excitation frequency in the sub-terahertz regime and are consistent with an extrapolation to zero in the limit of zero frequency. Qualitatively, this frequency dependence is reminiscent of the behaviour of the relaxation rate as a function of energy for a metal, in the sense that they go to zero as $\omega \to 0$ (for example, as $E \to E_F$) as the phase space for electronic relaxation collapses. However, the quantitative dependence is different as the relaxation rates are linear in frequency with a slope close to unity. We also find that the doping dependence (Fig. 3c) is such that the relaxation rates decrease as we approach the transition to the metallic phase. Figure 4 shows the temperature dependence of the relaxation rates. Over a range of temperatures from 5 K to 25 K, $1/T_2$ does not change at all to within experimental uncertainty, while the $1/T_1$ relaxation rate actually decreases with increasing temperature.

What can be inferred from these results? The temperature dependence in Fig. 4 and the frequency dependence in Fig. 3 rule out phonons as a dominant relaxation channel. Relaxation from phonons is known[34] to lead to relaxation rates that are increasing functions of temperature and with frequency dependence (Supplementary Section IV) that goes as ω^3 at low ω. The electronic system can thus be considered well isolated on the timescales of interest, with coupling to phonons unimportant for this relaxation. One can also rule out relaxation through coupling to magnetic excitations. At the energy scales of interest, magnetic excitations are tightly localized and do not form a heat bath[35] (Supplementary Section IV).

We further note that the temperature dependence of the energy relaxation rate $1/T_1$ (Fig. 4a) has the opposite sign from what one might naively expect—the relaxation rate decreases as we increase the temperature. This also rules out explanations based on spectral diffusion, but can be naturally explained if we postulate that T_1 comes from the interaction-mediated coherent tunnelling of electron–hole

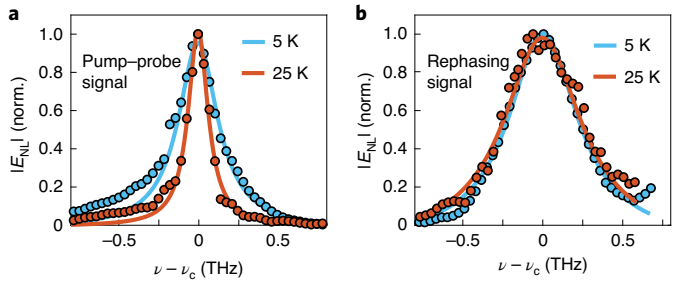

Fig. 4 | Temperature dependence of the pump–probe and rephasing anti-diagonal spectra. a, $|E_{NL}|$ as a function of frequency along the anti-diagonal cut of the PP signal in the first quadrant at $T = 5$ K and $T = 25$ K for the 39% sample. **b**, $|E_{NL}|$ as a function of frequency along the anti-diagonal cut of the R signal in the fourth quadrant at $T = 5$ K and $T = 25$ K for the 39% sample.

excitations (Supplementary Section IV). Raising the temperature increases screening and suppresses coherent tunnelling[36].

The doping dependence of the relaxation rate (Fig. 3c) provides further insight. This behaviour is counterintuitive: relaxation slows as we approach the metallic phase. We argue that, in fact, it is evidence that electron–electron interactions dominate relaxation. This follows from essentially dimensional considerations. Microscopically, the system consists of randomly placed phosphorus atoms. Electrons hop between these atoms, and repel each other via the Coulomb interaction. The system is doped toward the MIT by increasing the density of phosphorus atoms. Because the hopping is exponentially suppressed in the P–P distance and the Coulomb interactions are only algebraically suppressed, increasing the density decreases the ratio of interactions to hopping, and thus makes the system effectively more weakly interacting, causing the quasiparticle lifetimes to increase.

The linear-in-frequency relaxation rate with a slope close to unity is a dependence reminiscent of strongly correlated metals that exhibit the marginal Fermi liquid phenomenology[37,38]. Here it demonstrates something similar, with particle–hole excitations only marginally well defined in the relevant frequency range. By analogy with the 'marginal Fermi liquid', we dub the phase characterized by our experiments a 'marginal Fermi glass'. That the relaxation rates appear to extrapolate to zero in the zero frequency limit of the present case, despite the fact that the system is at finite temperature, probably reflects the fact that we are probing energy scales larger than the thermal scale. The smallest frequency probed (~0.5 THz) corresponds to a temperature of ~24 K, and the data in Fig. 3a are taken at 5 K. It is likely that the relaxation rates saturate to a non-zero value at a frequency lower than we can probe due to the finite temperature of the experiment.

We now sketch a mechanism that can give the linear-in-ω dependence (details are provided in Supplementary Section IV). The low-frequency excitations above the localized state are resonant particle–hole excitations, in which a particle is moved between two nearby localized orbitals. These excitations are local electric dipoles, and thus naturally interact via $1/R^3$ dipole–dipole interactions[15,39]. As discussed by Levitov[40], dipolar interactions are known to cause delocalization in three dimensions. Coulomb interactions parametrically enhance the density of dipoles at low frequencies[25], through a blockade effect; even if two nearby sites have on-site energies below E_F, occupying one of them may push the other site above E_F. These local anticorrelations among occupation numbers give a phase space of particle–hole excitations that is ω-independent at low frequencies (cf. Fermi liquids, where this phase space scales as ω). A dipolar excitation can coherently hop on this network, at a rate one can calculate (Supplementary Section IV) to be $\sim\omega$. This mechanism also has temperature and doping dependence consistent with the earlier dimensional analysis. It is important to point out that our experiment is not in the regime far from the MIT where the Shklovskii–Efros–Levitov calculation is well controlled. Nevertheless, it remains possible that the experimental results are quantitatively explicable via some non-trivial extension of its central ideas to systems near the MIT. Regardless of the precise mechanism, the relaxation comes from the interplay of strong electron–electron interactions with strong disorder, in a regime where controlled analytic calculation does not appear feasible. It should be noted that, in the absence of the Efros–Shklovskii ground-state reconstruction[25], the Levitov argument[40] would predict relaxation rates that scale as $\sim\omega^2$, implying sharply defined low-energy excitations (Supplementary Section IV). One needs both it and the long-range dipolar interaction to get the linear-in-ω relaxation.

Finally, we note that, although discussions of Fermi liquid theory are usually couched in terms of the lifetime of single electrons 'injected' above a filled Fermi sea, the lifetimes we are measuring here are those of elementary 'dipoles' (particle–hole excitations). In a Fermi liquid, these relaxation rates scale the same way; in disordered systems, they generally do not (Supplementary Section IV). Nevertheless, in the microcanonical ensemble (relevant for optical experiments, where we do not inject particles), particle–hole excitations are the low-energy excitations of the system, and the marginality of their lifetime is the key diagnostic of the marginal Fermi glass. Note that, although an anomalous particle–hole lifetime is sufficient to establish a 'non-Fermi glass', it is not necessary. We note that some proposed non-Fermi glasses[41] can have conventional particle–hole properties and only reveal their non-quasiparticle properties in their single-particle response, for example, via particle injection. Irrespective of these issues, the 'marginal Fermi glass' constitutes a distinct phenomenology and shows that interactions must be manifestly taken into account to describe these systems.

Online content

Any methods, additional references, Nature Research reporting summaries, source data, extended data, supplementary information, acknowledgements, peer review information; details of author contributions and competing interests; and statements of data and code availability are available at https://doi.org/10.1038/s41567-020-01149-0.

Received: 21 May 2020; Accepted: 11 December 2020;
Published online: 18 January 2021

References

1. Nozieres, P. *Theory of Quantum Liquids* (CRC Press, 2018).
2. Anderson, P. W. Absence of diffusion in certain random lattices. *Phys. Rev.* **109**, 1492–1505 (1958).
3. Abrahams, E. *50 Years of Anderson Localization* (World Scientific, 2010).
4. Anderson, P. W. *The Fermi Glass: Theory and Experiment* (World Scientific, 2004).
5. Efros, A. L. & Shklovskii, B. I. Coulomb gap and low temperature conductivity of disordered systems. *J. Phys. C* **8**, L49–L51 (1975).
6. Fleishman, L. & Anderson, P. Interactions and the Anderson transition. *Phys. Rev. B* **21**, 2366–2377 (1980).
7. Freedman, R. & Hertz, J. Theory of a Fermi glass. *Phys. Rev. B* **15**, 2384–2398 (1977).
8. Gornyi, I. V., Mirlin, A. D. & Polyakov, D. G. Interacting electrons in disordered wires: Anderson localization and low-T transport. *Phys. Rev. Lett.* **95**, 206603 (2005).
9. Basko, D. M., Aleiner, I. L. & Altshuler, B. L. Metal–insulator transition in a weakly interacting many-electron system with localized single-particle states. *Ann. Phys.* **321**, 1126–1205 (2006).
10. Nandkishore, R. & Huse, D. A. Many-body localization and thermalization in quantum statistical mechanics. *Annu. Rev. Condens. Matter Phys.* **6**, 15–38 (2015).
11. Abanin, D. A., Altman, E., Bloch, I. & Serbyn, M. Colloquium: many-body localization, thermalization and entanglement. *Rev. Mod. Phys.* **91**, 021001 (2019).

12. Burin, A. L., Kagan, Y., Maksimov, L. A. & Polishchuk, I. Y. Dephasing rate in dielectric glasses at ultralow temperatures. *Phys. Rev. Lett.* **80**, 2945–2948 (1998).
13. Burin, A. L. Energy delocalization in strongly disordered systems induced by the long-range many-body interaction. Preprint at https://arxiv.org/pdf/cond-mat/0611387.pdf (2006).
14. Yao, N. Y. et al. Many-body localization in dipolar systems. *Phys. Rev. Lett.* **113**, 243002 (2014).
15. Gutman, D. B. et al. Energy transport in the Anderson insulator. *Phys. Rev. B* **93**, 245427 (2016).
16. Nandkishore, R. M. & Sondhi, S. L. Many-body localization with long-range interactions. *Phys. Rev. X* **7**, 041021 (2017).
17. Woerner, M., Kuehn, W., Bowlan, P., Reimann, K. & Elsaesser, T. Ultrafast two-dimensional terahertz spectroscopy of elementary excitations in solids. *New J. Phys.* **15**, 025039 (2013).
18. Lu, J. et al. Coherent two-dimensional terahertz magnetic resonance spectroscopy of collective spin waves. *Phys. Rev. Lett.* **118**, 207204 (2017).
19. Wan, Y. & Armitage, N. Resolving continua of fractional excitations by spinon echo in THz 2D coherent spectroscopy. *Phys. Rev. Lett.* **122**, 257401 (2019).
20. Rosenbaum, T. et al. Metal–insulator transition in a doped semiconductor. *Phys. Rev. B* **27**, 7509–7523 (1983).
21. Paalanen, M., Rosenbaum, T., Thomas, G. & Bhatt, R. N. Critical scaling of the conductance in a disordered insulator. *Phys. Rev. Lett.* **51**, 1896–1899 (1983).
22. Helgren, E., Armitage, N. P. & Grüner, G. Frequency-dependent conductivity of electron glasses. *Phys. Rev. B* **69**, 014201 (2004).
23. Helgren, E., Armitage, N. P. & Grüner, G. Electrodynamics of a Coulomb glass in n-type silicon. *Phys. Rev. Lett.* **89**, 246601 (2002).
24. Lee, M. & Stutzmann, M. L. Microwave ac conductivity spectrum of a Coulomb glass. *Phys. Rev. Lett.* **87**, 056402 (2001).
25. Shklovskii, B. & Efros, A. Phononless hopping conduction in disordered systems. *Zh. Eksp. Theor. Fiz.* **81**, 406–415 (1981).
26. Mukamel, S. *Principles of Nonlinear Optical Spectroscopy* (Oxford Univ. Press, 1995).
27. Hamm, P. & Zanni, M. *Concepts and Methods of 2D Infrared Spectroscopy* (Cambridge Univ. Press, 2011).
28. Aue, W., Bartholdi, E. & Ernst, R. R. Two-dimensional spectroscopy. Application to nuclear magnetic resonance. *J. Chem. Phys.* **64**, 2229–2246 (1976).
29. Cundiff, S. T. & Mukamel, S. Optical multidimensional coherent spectroscopy. *Phys. Today* **66**, 44–49 (2013).
30. Kuehn, W., Reimann, K., Woerner, M., Elsaesser, T. & Hey, R. Two-dimensional terahertz correlation spectra of electronic excitations in semiconductor quantum wells. *J. Phys. Chem. B* **115**, 5448–5455 (2011).
31. Lu, J. et al. Nonlinear two-dimensional terahertz photon echo and rotational spectroscopy in the gas phase. *Proc. Natl Acad. Sci. USA* **113**, 11800–11805 (2016).
32. Choi, W., Lee, K. H. & Kim, Y. B. Theory of two-dimensional nonlinear spectroscopy for the Kitaev spin liquid. *Phys. Rev. Lett.* **124**, 117205 (2020).
33. Tomakoff, A. *Nonlinear and Two-Dimensional Spectroscopy* (Univ. Chicago, 2011); http://tdqms.uchicago.edu/page/nonlinear-and-two-dimensional-spectroscopy-notes
34. Galperin, Y., Gurevich, V. & Parshin, D. in *Hopping Transport in Solids* (eds Pollak, M. & Shklovskii, B) Ch. 3, 81–123 (Modern Problems in Condensed Matter Sciences Vol. 28, Elsevier, 1991).
35. Bhatt, R. N. & Lee, P. A. Scaling studies of highly disordered spin-1/2 antiferromagnetic systems. *Phys. Rev. Lett.* **48**, 344–347 (1982).
36. Fisher, M. P. A. & Zwerger, W. Quantum Brownian motion in a periodic potential. *Phys. Rev. B* **32**, 6190–6206 (1985).
37. Varma, C., Nussinov, Z. & van Saarloos, W. Singular or non-Fermi liquids. *Phys. Rep.* **361**, 267–417 (2002).
38. Varma, C., Littlewood, P. B., Schmitt-Rink, S., Abrahams, E. & Ruckenstein, A. Phenomenology of the normal state of Cu–O high-temperature superconductors. *Phys. Rev. Lett.* **63**, 1996–1999 (1989).
39. Burin, A. & Kagan, Y. Low-energy collective excitations in glasses. New relaxation mechanism for ultralow temperatures. *Zh. Eksp. Teor. Fiz.* **106**, 633–647 (1994).
40. Levitov, L. S. Absence of localization of vibrational modes due to dipole–dipole interaction. *Europhys. Lett.* **9**, 83–86 (1989).
41. Parameswaran, S. A. & Gopalakrishnan, S. Non-Fermi glasses: localized descendants of fractionalized metals. *Phys. Rev. Lett.* **119**, 146601 (2017).

Methods

Experiments were performed on nominally uncompensated phosphorous-doped silicon (Si:P) samples, which were cut from a Czochralski-grown boule to a specification of 5 cm in diameter with a phosphorus-dopant gradient along the axis. This boule was subsequently sliced and then polished down to 100-μm wafers. Samples from this boule were previously used for studies of terahertz-range conductivity in the phononless regime[22,23] and optical pump–terahertz probe measurements[42]. We measured samples from 39 to 85% of the critical concentration of the 3D MIT in a regime where the localization length was of order or longer than the inter-dopant spacing. Note that these concentrations are far higher than those used in terahertz free electron laser (FEL) studies demonstrating photon echo at the $1s \rightarrow 2p_0$ transition (~8.29 THz)[43,44]. The phosphorus concentrations were calibrated with room-temperature resistivity using the Thurber scale[45].

To perform 2D nonlinear terahertz spectroscopy, two intense terahertz pulses (A and B) generated by the tilted pulse front technique and separated by a time-delay τ (Fig. 1b) were focused onto each sample in a collinear geometry (see Supplementary Section I for details of the experimental set-up)[17,18]. The transmitted terahertz fields were detected by standard electro-optic (EO) sampling using a 30-fs, 800-nm pulse delayed by time t relative to pulse B. The displayed data were taken with a maximum electric field of 50 kV cm^{-1} for each pulse. A differential chopping scheme was used to extract the nonlinear signal ($E_{\mathrm{NL}}(\tau,t) = E_{\mathrm{AB}}(\tau,t) - E_{\mathrm{A}}(\tau,t) - E_{\mathrm{B}}(t)$) resulting from the interaction of the two terahertz pulses with the sample. Here, E_{AB} is the transmitted signal when both terahertz pulses are present, while E_{A} and E_{B} are the transmitted signals with each pulse A and B present individually. A 2D Fourier transform of E_{NL} with respect to τ and t gives the complex 2D spectra as a function of the frequency variables ν_τ and ν_t. Fits to Lorentzians were restricted to the central part of peaks due to the phase twisting present in these spectra, as discussed in Supplementary Section III.

Data availability

All data that support the plots within this paper and other findings of this study are available from the corresponding author upon reasonable request.

References

42. Thorsmølle, V. & Armitage, N. Ultrafast (but many-body) relaxation in a low-density electron glass. *Phys. Rev. Lett.* **105**, 086601 (2010).
43. Greenland, P. et al. Coherent control of Rydberg states in silicon. *Nature* **465**, 1057–1061 (2010).
44. Lynch, S. A. et al. First observation of a THz photon echo. In *35th International Conference on Infrared, Millimeter and Terahertz Waves* 1–2 (IEEE, 2010).
45. Thurber, W. R., Mattis, R. L., Liu, Y. M. & Filliben, J. J. Resistivity-dopant density relationship for phosphorus-doped silicon. *J. Electrochem. Soc.* **127**, 1807–1812 (1980).

Acknowledgements

We thank A. Burin, Y. Galperin, Y.-B. Kim, A. Legros, I. Martin, A. Millis, V. Oganesyan, S. Parameswaran, B. Shklovskii and Y. Yuan for helpful discussions. This project was supported by a now-cancelled DARPA DRINQS programme grant and by the Gordon and Betty Moore Foundation, EPiQS initiative, grant number GBMF-9454. S.G. acknowledges support from NSF grant no. DMR-1653271.

Author contributions

F.M. and D.C. built the 2D terahertz set-up and carried out experiments and analysis. S.G. and R.N. provided theoretical support. N.P.A. directed the project. All authors contributed to the writing and editing of the manuscript.

Competing interests

The authors declare no competing interests.

Additional information

Supplementary information is available for this paper at https://doi.org/10.1038/s41567-020-01149-0.

Correspondence and requests for materials should be addressed to F.M. or N.P.A.

Peer review information *Nature Physics* thanks the anonymous reviewers for their contribution to the peer review of this work.

Reprints and permissions information is available at www.nature.com/reprints.